

Training Medical Large Vision-Language Models with Abnormal-Aware Feedback

Yucheng Zhou Lingran Song Jianbing Shen*

SKL-IOTSC, CIS, University of Macau

yucheng.zhou@connect.um.edu.mo, jianbingshen@um.edu.mo

Abstract

Existing Medical Large Vision-Language Models (Med-LVLMs), which encapsulate extensive medical knowledge, demonstrate excellent capabilities in understanding medical images and responding to human queries based on these images. However, there remain challenges in visual localization in medical images, which is crucial for abnormality detection and interpretation. To address these issues, we propose a novel UMed-LVLM designed with Unveiling Medical abnormalities. Specifically, we collect a Medical Abnormalities Unveiling (MAU) dataset and propose a two-stage training method for UMed-LVLM training. To collect MAU dataset, we propose a prompt method utilizing the GPT-4V to generate diagnoses based on identified abnormal areas in medical images. Moreover, the two-stage training method includes Abnormal-Aware Instruction Tuning and Abnormal-Aware Rewarding, comprising Abnormal Localization Rewarding and Vision Relevance Rewarding. Experimental results demonstrate that our UMed-LVLM surpasses existing Med-LVLMs in identifying and understanding medical abnormality. In addition, this work shows that enhancing the abnormality detection capabilities of Med-LVLMs significantly improves their understanding of medical images and generalization capability.

1 Introduction

Large Vision-Language Models (LVLMs) demonstrate remarkable capability in various vision-language tasks (OpenAI, 2023a; Liu et al., 2023b; Li et al., 2023a). Medical image analysis poses a significant challenge for LVLMs due to their intricate patterns and structures, thereby demanding an in-depth grasp of nuanced variations to ensure precise diagnoses (Wu et al., 2023). To enhance LVLMs for medical images, some works (Qin et al., 2023) encapsulate a substantial medical corpus into

Table 1: Comparison of different Med-LVLMs: RegionGPT (Guo et al., 2024), XrayGPT (Thawakar et al., 2023), Med-Flamingo (Moor et al., 2023), MedVInt (Zhang et al., 2023a) and Ours. “Medical Diagnosis” denotes the model’s applicability for medical diagnosis; “Multi-modal Medical Image” indicates training on multi-modal medical images; “Region-Awareness” reflects the model’s capability for region recognition; “Detector & Segmenter-Free” specifies independence from external detectors or segmenters.

Method	Medical Diagnosis	Multi-modal Medical Image	Region-Awareness	Detector & Segmenter-Free
RegionGPT	✓	✗	✓	✗
XrayGPT	✓	✗	✗	✓
Med-Flamingo	✓	✓	✗	✓
MedVInt	✓	✓	✗	✓
Our UMed-LVLM	✓	✓	✓	✓

these models, i.e., Medical Large Vision-Language Models (Med-LVLMs). These Med-LVLMs exhibit proficiency in understanding medical images and human queries.

Despite their successes, existing Med-LVLMs exhibit limitations in visual localization capability within medical images, as shown in Table 1. Advanced models like GPT-4V (OpenAI, 2023a), one of the leading LVLMs, exhibit notable shortcomings in accurately interpreting and visual localization in medical images (i.e., abnormality localization) (Wu et al., 2023). The capability for visual localization is critical for two primary reasons: Firstly, bias in visual localization can lead to unreliable responses in diagnosis, undermining the credibility and interpretability of Med-LVLMs. Secondly, some LVLMs (Yin et al., 2023; Guo et al., 2024; Ranasinghe et al., 2024) improve the visual understanding in LVLM by enhancing its visual localization capability. In these works, visual localization in natural scenes can benefit from general detectors. However, abnormality localization in medical images lacks a large number of data to train specialized detectors, especially for some rare diseases. This limitation emphasizes the necessity for enhancing the inherent visual localization capabilities of medical LVLMs without specific detectors to improve their understanding of medical images and the reliability of responses.

*Corresponding Authors.

To address these challenges, we propose **UMed-LVLM**, designed with **Unveiling Medical** abnormalities for **LVLM**. To encapsulate abnormality unveiling capability into UMed-LVLM, we first collect a dataset comprising medical images with abnormality regions. Then, we design a prompt method to generate a diagnosis dataset, i.e., Medical Abnormalities Unveiling (MAU), through the GPT-4V model (OpenAI, 2023b). The MAU dataset encompasses medical images, user queries, and diagnosis responses with abnormal areas. This dataset is utilized to train UMed-LVLM via a two-stage training method, i.e., Abnormal-Aware Instruction Tuning and Abnormal-Aware Rewarding, enabling it to understand medical abnormalities. The Abnormal-Aware Rewarding strategy, comprising Abnormal Localization Rewarding and Vision Relevance Rewarding, aims to improve the model’s capability to capture abnormal areas.

In the experiments, we evaluate UMed-LVLM and other methods on MAU dataset, and UMed-LVLM outperforms other competitors in understanding medical images and identifying abnormalities. Moreover, an in-depth analysis revealed that while Med-LVLMs are not yet adept at abnormality detection in medical images, enhancing their abnormality detection capabilities can improve their understanding of medical images. Furthermore, our findings suggest that large models possess out-of-distribution (OOD) generalization capabilities, indicating the potential for more robust disease recognition through iterative improvements in large models, even if they are only exposed to diverse medical images of limited disease types (Zhang et al., 2021). In addition, we analyze the cross-modal capabilities and generalization potential of Med-LVLMs, and results show that augmenting models in varied modalities enhances their performance in modality with limited dataset availability.

There are the main contributions of this work:

- We propose a novel UMed-LVLM, for medical diagnosis with unveiling abnormality. It aims to enhance the visual localization capability of Med-LVLMs to improve their medical image understanding.
- We introduce Abnormal-Aware Instruction Tuning and Abnormal-Aware Rewarding strategy to train the Med-LVLM, aiming to enhance the model’s focus on abnormal areas when generating responses.
- We design a prompt method to create the

MAU dataset for UMed-LVLM training. The dataset comprises medical images and diagnoses with abnormalities annotations.

- Experimental results show that UMed-LVLM outperforms existing Med-LVLMs in identifying and understanding medical abnormalities. We conduct an in-depth analysis of model training and generalization capabilities, underscoring the potential of incorporating medical abnormalities to enhance Med-LVLM.

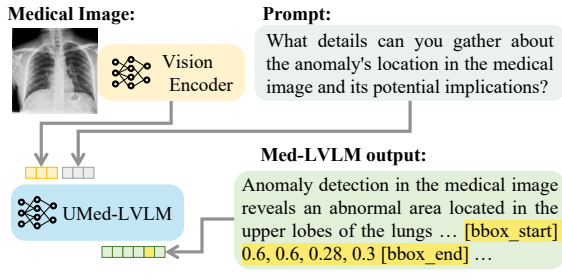
2 Related Work (summarized)

Recent advancements in LVLMs have significantly improved visual comprehension and contextual language understanding (Alayrac et al., 2022; Chen et al., 2023; Zhou et al., 2024a). Notable models like CLIP (Radford et al., 2021) and BLIP-2 (Li et al., 2023b) have achieved impressive results in vision-language tasks by leveraging pre-trained image-text pairs. The introduction of GPT-4 (OpenAI, 2023a) has further propelled this field, with models like LLaVA (Liu et al., 2023b) and its improved version (Liu et al., 2023a) demonstrating exceptional capabilities in multimodal tasks. In the medical domain, models such as LLaVA-Med (Li et al., 2023a), Visual Med-Alpaca (Shu et al., 2023), OphGLM (Gao et al., 2023), and XrayGPT (Thawakar et al., 2023) have specialized in interpreting medical images and providing comprehensive assistance. Observations in (Wu et al., 2023) indicated that although GPT-4V performs well in differentiating medical image modalities and anatomy, it still has difficulties in disease diagnosis and generating comprehensive reports. Additionally, Reinforcement Learning (RL) has been applied to LLMs to enhance their performance and flexibility (Sutton and Barto, 1998; Mnih et al., 2015; Schulman et al., 2015; Mnih et al., 2016; Schulman et al., 2017). Successful implementations include WebGPT (Nakano et al., 2021) and InstructGPT (Stiennon et al., 2020; Christiano et al., 2017; Brown et al., 2020), which use RL to optimize behavior and follow instructions. The full version can be found in Appendix A.

3 Methodology

In this study, we train UMed-LVLM with a two-stage training method, i.e., Abnormal-Aware Instruction Tuning and Abnormal-Aware Rewarding. Abnormal-Aware Rewarding comprises a LLM relevance reward model and two rewarding strategies,

Step 1: Abnormal-Aware Instruction Tuning



Step 2: Fine-tune the policy UMed-LVLM against the Abnormal-Aware Rewarding using RL

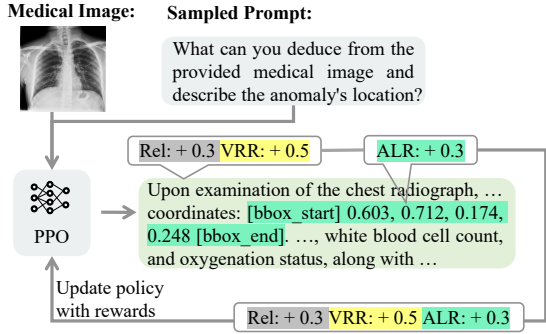


Figure 1: The two-stage training for our UMed-LVLM. “Rel”, “VRR” and “ALR” denote “Relevance Reward”, “Abnormal Localization Reward” and “Vision Relevance Reward”, respectively, as detailed in Sec. 3.2.

i.e., Abnormal Localization Rewarding and Vision Relevance Rewarding.

3.1 Abnormal-Aware Instruction Tuning

To improve task adaptability, accuracy, and efficiency in LVLMs, Liu et al. (2023b) employ Instruction Tuning (Wei et al., 2022). This approach enhances the model’s ability to understand and follow instructions effectively. To enhance our model’s capability to understand medical abnormal regions and generate corresponding diagnoses with abnormal regions, we perform Abnormal-Aware Instruction Tuning on UMed-LVLM.

Specifically, given a medical image x and a user query q , our model generates a response a containing the abnormal region and diagnosis through autoregressive decoding, i.e.,

$$p(a|x, q; \theta) = \prod_{t=1}^T p(a_t|a_{<t}, x, q; \theta), \quad (1)$$

where $a_{<t}$ represents the first t tokens of a , T is the length of the response, and θ denotes the model parameters. The model predicts the next token based on the preceding t tokens until the complete response is generated.

In model training, we input medical images x , user queries q , and the diagnosis responses a with corresponding abnormal regions, computing the probability of the model-generated response a , i.e.,

$$h_i = \text{Med-LVLM}(x, q, a_{<i}; \theta), i \in \{1, 2, \dots, T\} \quad (2)$$

where $mlvlm$ is our model, θ are the model parameters, T is the length of the ground truth response a , and h_i is the hidden state of the i -th token in the model-generated response a . The softmax function calculates the probability distribution over the vocabulary of generating each token:

$$p_i = \text{softmax}(Wh_i + b), \quad (3)$$

where W and b are the parameters of the language model head, and p_i is the probability of the i -th token in response a . We optimize the model parameters using the cross-entropy loss function:

$$\mathcal{L}_{it} = - \sum_{i=1}^T \log p_i. \quad (4)$$

This approach improves the model’s understanding of abnormal regions in medical images and its ability to provide diagnosis outputs with identified abnormal regions and categories. However, it does not directly guide the model to focus on abnormal regions in medical images.

3.2 Abnormal-Aware Rewarding

To address the challenge of effectively identifying and describing abnormalities within medical images, we propose an Abnormal-Aware Rewarding (AAR) strategy for UMed-LVLM training. This reinforcement learning (RL) training strategy comprises a LLM relevance reward model and two rewarding strategies, i.e., Abnormal Localization Rewarding and Vision Relevance Rewarding, designed to optimize the Med-LVLMs based on abnormalities. In contrast to Ouyang et al. (2022) optimize LLMs following user instructions by the Proximal Policy Optimization (PPO (Schulman et al., 2017)), AAR optimizes the Med-LVLMs by a more directed learning towards the accurate medical diagnosis with abnormality recognition.

3.2.1 LLM Relevance rewarding

The LLM relevance rewarding framework is fundamentally structured around three pivotal components: the policy network, the value network and the LLM reward model. Both networks play a crucial role in guiding the training process, with the

policy network (π) generating actions (responses) based on the given state s_t , which encapsulates the medical image x and user query q . The policy network’s output is mathematically expressed as:

$$\pi(a_t|s_t; \theta) = \prod_{t=1}^T \pi(a_t|s_t, a_{<t}; \theta), \quad (5)$$

where θ denotes the parameters of policy network.

Simultaneously, the value network (V) is tasked with estimating the expected return from state s_t , offering an essential benchmark for calculating the advantage function crucial for the policy network’s optimization:

$$V(s_t; \phi) = \mathbb{E}[r_t | s_t, \pi], \quad (6)$$

where ϕ represents the parameters of the value network, and r_t denotes the immediate reward associated with the current state s_t .

The LLM relevance rewarding framework incorporates rewards from the policy network, the value network, and the LLM relevance reward model. The total reward, $r_t^{\pi, V, LLM}$, measures the improvement of the chosen action over the baseline provided by the value network and includes the relevance reward from the LLM model:

$$r_t^{\pi, V, LLM} = A(s_t, a_t; \theta, \phi) + r_t^{LLM}, \quad (7)$$

where $A(s_t, a_t; \theta, \phi) = Q(s_t, a_t; \theta) - V(s_t; \phi)$ is the advantage function, and r_t^{LLM} represents the relevance reward provided by the LLM model. The Q-function $Q(s_t, a_t; \theta)$ is updated using the Bellman equation:

$$\Delta Q(s_t, a_t) = \alpha \left[r_t + \gamma \max_{a'} Q(s_{t+1}, a') - Q(s_t, a_t) \right], \quad (8)$$

$$Q(s_t, a_t) \leftarrow Q(s_t, a_t) + \Delta Q(s_t, a_t), \quad (9)$$

where α is the learning rate, r_t is the immediate reward, γ is the discount factor, and $\max_{a'} Q(s_{t+1}, a')$ is the maximum expected future reward for the next state s_{t+1} .

3.2.2 Abnormal Localization Reward

The Abnormal Localization Reward (ALR) is calculated by Intersection over Union (IoU) scores between the generated and ground truth bounding boxes. Specifically, the ALR (r_t^{loc}) is derived from the IoU score, which quantitatively measures the

accuracy of the predicted bounding boxes against the ground truth one:

$$r_t^{loc} = \text{IoUScore}(\text{PredBBox}, \text{GTBBox}), \quad (10)$$

where PredBBox and GTBBox represent the predicted and ground truth bounding boxes, respectively. The IoUScore is calculated as follows:

$$\text{IoUScore}(x_1, x_2) = \frac{\text{Overlap}(x_1, x_2)}{\text{Union}(x_1, x_2)}, \quad (11)$$

this function quantifies the overlap between the predicted and ground truth bounding boxes, providing a measure of localization accuracy.

3.2.3 Vision Relevance Reward

The Vision Relevance Reward (VRR) is computed by the assigned attention weights between abnormal category tokens assigned and abnormal areas in the image. Specifically, the VRR, r_t^{att} , is determined by analyzing the attention mechanisms within a transformer framework. This reward is calculated based on the attention scores allocated to tokens that correspond to the abnormal categories, with a specific focus on the image patches indicative of abnormal regions. The computation is designed to enhance the model’s ability to concentrate on crucial visual areas, thereby improving its diagnosis accuracy:

$$r_t^{att} = \sum_{i \in N} \sum_{j \in \bar{N}} \text{ATTN}(i, j), \quad (12)$$

where N denotes the set of tokens that are directly associated with identified abnormalities within the text, and \bar{N} refers to the patches of the image that are characterized as abnormal regions. The $\text{ATTN}(i, j)$ represents the weight attributed to the i -th token for its relevance to the j -th abnormal region patch. The detailed calculation of $\text{ATTN}(i, j)$ is as follows:

$$\text{score}_{i,j} = \frac{Q_i \cdot K_j^\top}{\sqrt{d_k}}, \quad (13)$$

$$\text{ATTN}(i, j) = \frac{\exp(\text{score}_{i,j})}{\sum_{k \in \bar{N}} \exp(\text{score}_{i,k})}, \quad (14)$$

where Q_i is the query vector for token i , and K_j is the key vector for image patch j ; d_k and \bar{N} are the dimensionality of the key vectors and the set of all abnormal image patches. This approach allows us to quantify the model’s focus on critical areas by leveraging the transformer’s inherent attention

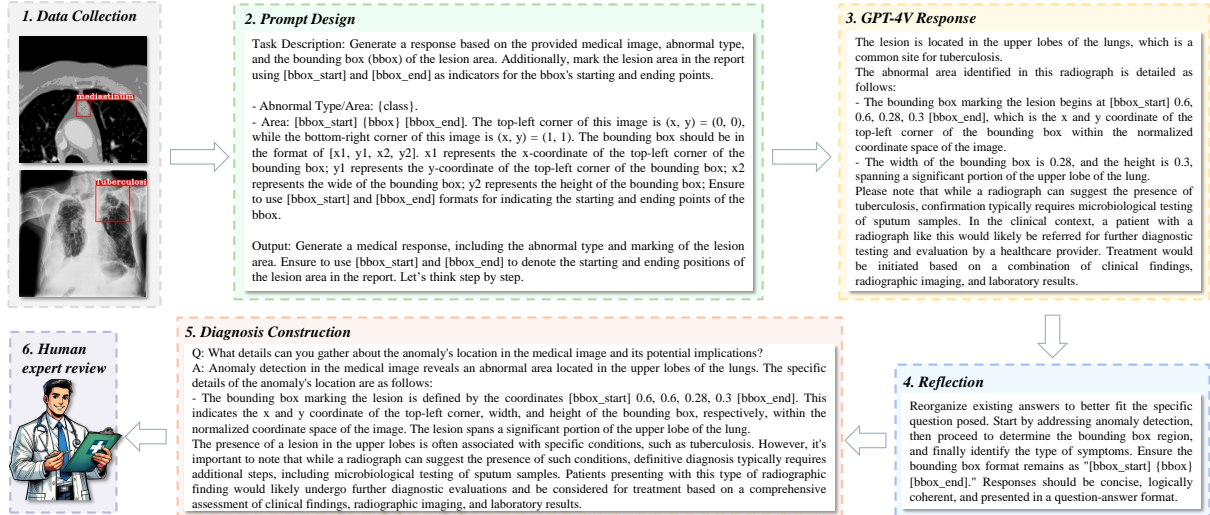


Figure 2: Pipeline overview for constructing the medical abnormalities unveiling (MAU) dataset. The process involves data collection, prompt design, GPT-4V response generation, reflection for outputs, diagnosis construction, and human expert review.

mechanism. By emphasizing the importance of tokens related to abnormalities and their corresponding weights over the abnormal patches of the image, we ensure that the model rewards attention that accurately reflects the presence and significance of medical abnormalities.

3.2.4 Reward Normalization and Aggregation

To achieve equilibrium between the ALR (r_t^{loc}) and the VRR (r_t^{att}), we individually normalize these rewards for responses generated by the same query. This normalization ensures that each reward type contributes equally to the final reward calculation. The combined reward for each response is computed as follows:

$$r_t = r_t^{\pi, V, LLM} + \frac{r_t^{loc}}{\max(r_t^{loc})} + \frac{r_t^{att}}{\max(r_t^{att})}, \quad (15)$$

where $\max(r_t^{loc})$ and $\max(r_t^{att})$ are the maximum values of the abnormal-aware localization and attention reward, respectively, for all responses to a particular query.

3.2.5 Optimization Process

As an improved version of the PPO framework, our policy network is refined by maximizing an objective function that incorporates the combined reward r_t into the PPO framework. Specifically, we aim to maximize an objective function that combines the clipped surrogate objective with an entropy bonus to encourage exploration:

$$\mathcal{L}^{\text{CLIP+ENT}}(\theta) = \hat{\mathbb{E}} \left[\mathcal{L}^{\text{CLIP}}(\theta) + c_1 r_t - c_2 \mathcal{L}^{VF}(\phi) + c_3 S[\pi(\cdot|s_t)] \right], \quad (16)$$

where $\mathcal{L}^{\text{CLIP}}(\theta)$ is the clipped part of the PPO objective, r_t is the combined normalized reward as defined previously, $\mathcal{L}^{VF}(\phi)$ is the value function loss, $S[\pi(\cdot|s_t)]$ denotes the entropy of the policy for state s_t , and c_1, c_2, c_3 are coefficients balancing the contribution of each term.

4 MAU Dataset

To enhance the abnormality unveiling capabilities of the Med-LVLM, we construct the MAU dataset for UMed-LVLM training. Firstly, we collect medical image datasets with abnormal annotations. Then, we design a Prompt Method to construct the MAU dataset, a medical diagnosis dataset with abnormal annotations, by GPT-4V (OpenAI, 2023b).

4.1 Collecting Medical Image Datasets with Abnormal Areas

We collect a medical image dataset annotated with abnormal areas for training the Med-LVLM. This dataset encompasses five distinct sub-datasets, namely DeepLesion (Yan et al., 2017), Kidney-Stone (TEZ, 2023), NIH (Wang et al., 2017), TBX11K (Liu et al., 2020), and KVASIR (Pogorelov et al., 2017), each originating from diverse sources. DeepLesion includes 32,120 axial CT slices with eight types of abnormalities. The KidneyStone dataset contains 1,300 renal CT scans of various kidney stones in different sizes, shapes, and locations. The NIH dataset has 112,120 chest X-ray images across 14 pathological categories. The TBX11K dataset consists of 11,200 chest X-ray images for tuberculosis detection. The KVASIR dataset provides 8,000 endoscopic im-

ages of the gastrointestinal tract, with eight types of abnormalities. These sub-datasets span various medical imaging modalities, including X-rays, CT scans, and gross pathology. We utilized a portion of these datasets, and Appendix B summarizes the specific details of the segments used from each sub-dataset. Each image is annotated with the type of abnormality present and includes bounding box information for identified abnormal areas.

4.2 Medical Abnormal Unveiling Dataset Construction

To construct the Medical Abnormal Unveiling (MAU) Dataset, we design a Prompt Method that utilizes the GPT-4V model to generate diagnosis annotations with medical abnormal areas. The pipeline, as shown in Figure 2, comprises two stages: diagnosing abnormalities in medical images and reflecting on the previous diagnosis. Firstly, we integrate collected medical images, corresponding abnormality categories, and the locations of abnormal areas into our designed prompt. This prompt is then passed into GPT-4V to generate diagnosis responses based on the given abnormality categories and areas. To build a diagnosis with step-by-step thoughts, a reflection prompt is designed to reorganize these diagnosis responses, starting from abnormality detection, identifying bounding box regions, and finally recognizing abnormality categories. The processed responses, the medical images, and queries form medical image diagnosis samples. Through this Prompt Method, we harness the GPT-4V model to generate the MAU dataset, and examples of the MAU dataset can be found in Appendix B. Our prompt method is plug-and-play, characterized by its ease of integration with other medical datasets and independence from disease-specific designs. To ensure the safety and reliability of the GPT-4V-generated diagnoses, all generated data have been reviewed and filtered by three doctoral students specializing in medicine.

5 Experiments

5.1 Experimental Setups

In our experiments, we evaluated our model on the test set of MAU data. Our dataset comprises five sub-datasets: DeepLesion, KidneyStone, NIH, TBX11K, and KVASIR. We utilized MedVInt, a vision-language model pre-trained extensively on medical knowledge, as the initialization for our model. To prevent knowledge catastrophic forget-

Table 2: Comparison on test set. “DL”, “KS” and “KV” denote “Deep Lesion”, “Kidney Stone” and “KVASIR”, respectively. GPT-4V is tested on 200 samples randomly sampled from the whole test set. The comparison models include LVLMS (i.e., MiniGPT-4 (Zhu et al., 2024), mPLUG-Owl (Ye et al., 2023), LLaVA (Liu et al., 2023b), Qwen-VL (Bai et al., 2023), GPT-4V (OpenAI, 2023b)) and Med-LVLMS (i.e., XrayGPT (Thawakar et al., 2023), LLaVA-Med (Li et al., 2023a), Med-Flamingo (Moor et al., 2023), MedVInt (Zhang et al., 2023a)). MedVInt* represents MedVInt trained with SFT on the MAU dataset, while MedVInt* denotes MedVInt trained with both SFT and PPO on the MAU dataset.

Method	DL	KS	KV	NIH	TBX	Avg.
MiniGPT-4	0.02	0.00	0.02	0.00	0.00	0.01
mPLUG-Owl	0.05	0.00	0.01	0.00	0.00	0.01
LLaVA	0.20	0.00	0.04	0.00	0.00	0.05
Qwen-VL	0.13	0.00	0.01	0.00	0.00	0.03
XrayGPT	0.18	0.12	0.02	0.07	0.06	0.09
LLaVA-Med	0.22	0.04	0.12	0.03	0.01	0.08
Med-Flamingo	0.27	0.15	0.15	0.09	0.02	0.14
MedVInt	0.29	0.11	0.27	0.08	0.09	0.17
<i>Trained on MAU Dataset</i>						
MedVInt*	0.42	0.93	0.93	0.28	0.78	0.67
MedVInt*	0.44	0.94	0.95	0.30	0.80	0.69
UMed-LVLM	0.53	0.99	0.98	0.37	0.86	0.75
GPT-4V	-	-	-	-	-	0.34

ting of large language model during continual training on large-scale datasets (Luo et al., 2023), we train the model on limited-scale datasets, following that employed in previous studies (Zhou et al., 2023; Yu et al., 2024). Therefore, UMed-LVLM is trained on the training set of 4,653 examples and then evaluated on 1,164 examples. For evaluation metrics, we utilized Accuracy (ACC) as evaluation metric. ACC assesses the correctness of diagnosis results, specifically whether the response text includes the correct category of abnormalities, similar to the method used in (Wu et al., 2024) to evaluate the correctness of outputs from LVLMS. In the experiments, we employ MedVInt (Zhang et al., 2023b) to initialize our model. The implementation details and details on LVLMS methods we compare can be found in Appendix C and Appendix D.

5.2 Results and Discussion

We compared the performance of our method with other LVLMS on the MAU dataset. As shown in Table 2, our method outperforms other methods across all datasets. This substantial lead is attributed to our model’s ability to integrate abnormal unveiling capabilities. Unlike other specific models, UMed-LVLM appears to more effectively generalize from the training data to the test scenarios, indicating critically valuable robustness in medical imaging applications where precision is paramount.

Table 3: Ablation study verifies the effectiveness of components in the Abnormal-Aware Rewarding (AAR), including two components: Abnormal Localization Reward (ALR) and Abnormal-Vision Relevance Reward (VRR). “w/o AAR” denotes UMed-LVLM only trained on Abnormal-Aware Instruction Tuning.

Method	DL	KS	KV	NIH	TBX	Avg.
UMed-LVLM	0.53	0.99	0.98	0.37	0.86	0.75
w/o VRR	0.49	0.97	0.95	0.30	0.82	0.71
w/o ALR	0.48	0.96	0.96	0.35	0.83	0.72
w/o AAR	0.42	0.93	0.93	0.28	0.78	0.67

By comparing UMed-LVLM with MedVInt* and MedVInt*, the performance gain can be attributed to the MAU dataset and our Abnormal-Aware Rewarding approach. In addition, the results show a direct comparison between UMed-LVLM and GPT-4V. The results of GPT-4 were conducted by a subset of 200 samples randomly selected from the entire test set. From the results, UMed-LVLM significantly outperforms GPT-4V. The results underline the enhanced capabilities of UMed-LVLM in medical image understanding. The case study can be found in Appendix E.

5.3 Ablation Study

To verify the efficacy of components in AAR, we conducted experiments by progressively removing each component from UMed-LVLM to observe the impact on performance. As shown in Table 3, we compare the performance of UMed-LVLM and its three variants, i.e., “w/o ALR”, “w/o VRR”, and “w/o AAR”. The results show a performance decline as components are removed, demonstrating that each component plays a critical role in enhancing diagnosis accuracy for medical images. From the table, we can observe that both ALR and VRR significantly contribute to the model’s performance. The VRR, by aligning abnormal identification and attention regions, ensures that the model does not overlook subtle but critical abnormalities in the images. On the other hand, the ALR component reinforces the abnormal localization, which is paramount in medical diagnosis. The performance degradation observed when either component is removed substantiates the hypothesis that a dual-reward system, which addresses abnormality recognition and localization, is beneficial in diagnosis.

5.4 Analysis

Impact of Abnormal Localization. To verify the impact of localization ability during the reason-

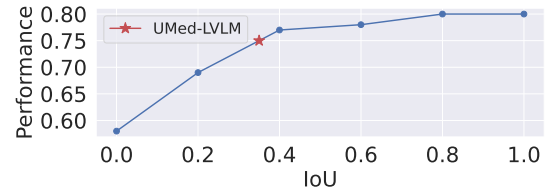


Figure 3: Performance of UMed-LVLM with different IoUs.

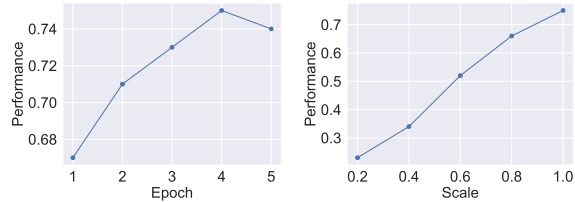


Figure 4: Performance of Abnormal-Aware Instruction Tuning across different epochs (Left) and data scales (Right).

ing process on Med-LVLM, we injected bounding boxes (bbox) corresponding to different IoU scores during model inference for observation. The experimental results, as shown in Figure 3, indicate that enhancing localization ability can influence the diagnostic results. As anomaly localization becomes more accurate, the model’s diagnostic performance improves. However, when IoU exceeds 0.6, the improvement in the model’s diagnostic performance begins to plateau. This suggests that Med-LVLM does not require extremely high localization accuracy to leverage the reasoning gains from localization; a certain level of localization ability is sufficient to enhance diagnostic reasoning. The red dot in the figure represents the performance achieved by our UMed-LVLM. From the trend, it is evident that the localization ability of our method effectively enhances model’s diagnostic capability.

Impact of Instruction Tuning Epoch. As shown in Figure 4(Left), we investigate the effects of employing Instruction Tuning over different epochs on the performance of our model. The performance exhibits an upward trajectory until epoch 4, achieving a peak of approximately 0.75, which suggests that the model becomes progressively more adept at executing tasks as per the user queries and medical image inputs. This improvement in performance underscores the model’s enhanced understanding of the medical abnormalities and its ability to generate correct responses.

Impact of Training Set Scale for Instruction Tuning. As shown in Figure 4(Right), the performance of our model exhibits a positive correlation with the scale of the training data. We can observe a substantial increment as the data scale progresses from 20% to 100%. This trend illus-

Table 4: Model generalization to categories excluded from training set. MedVInt \star and MedVInt \ast can be found in Table 2.

Method	Abdomen	Lung	Pelvis
UMed-LVLM	0.35	0.39	0.27
MedVInt \star	0.16	0.15	0.16
MedVInt \ast	0.15	0.12	0.15
MedVInt	0.05	0.04	0.07

Table 5: Performance of UMed-LVLM w/o training on TBX11K and DeepLesion datasets, respectively. Performance is evaluated on the excluded datasets.

Method	TBX11K	Deep Lesion
UMed-LVLM	0.57	0.42
MedVInt \star	0.29	0.28
MedVInt \ast	0.30	0.22
MedVInt	0.10	0.08

trates that the model benefits from a larger volume of data, refining its ability to understand abnormalities and execute instructions more effectively. This improvement underscores the model’s evolving proficiency in identifying the exact spatial extents of abnormalities, which is crucial for subsequent diagnosis tasks. The incremental nature of this trend indicates that the model’s spatial comprehension capabilities can be significantly honed with more extensive training data. These results collectively highlight the critical role that data scale plays in the efficacy of instruction tuning for Med-LVLM.

Generalization Capability for Un-trained Category. This setting aims to evaluate the generalization capability of the UMed-LVLM on medical categories not present in the training data. Specifically, we removed data in three categories (i.e., “Abdomen”, “Lung”, and “Pelvis” on “DeepLesion”) on the training set. Then we evaluated the trained model on these categories to observe its ability to handle un-trained categories. The results, shown in Table 4, present the performance in each category. The performance demonstrates that our method exhibits a degree of generalization capability on un-trained categories of medical images. Although the performance on un-trained categories is somewhat reduced compared to training on these categories, these findings indicate that the model can generalize knowledge learned during training to new categories not present in the training data. In contrast, MedVInt shows a slight ability to generalize to these un-trained categories with scores close to zero across all categories. This demonstrates that abnormal-aware learning is effective for Med-LVLM training.

Table 6: Cross-modal generalization capability models trained on single modality medical images. “C”, “G”, and “X” represent CT, Gross Pathology, and X-ray, respectively.

Method	C ->GX	G ->CX	X ->CG
UMed-LVLM	0.27	0.31	0.22
MedVInt \star	0.12	0.08	0.13
MedVInt \ast	0.09	0.08	0.11
MedVInt	0.05	0.04	0.07

Generalization Capability of Abnormality Unveiling.

To assess the robustness and flexibility of UMed-LVLM and MedVInt, we respectively removed the TBX11K and DeepLesion datasets from the training data to verify the models’ generalization capabilities. We evaluated the models on the excluded datasets to determine their ability to generalize across different medical datasets. As shown in Table 5, UMed-LVLM demonstrated significantly better generalization than other methods. The performance disparity underscores our model’s effectiveness in adapting to varied medical scenarios, indicating a robust learning framework is not only overfitted to training data but instead potential to handle diverse medical imaging challenges.

Generalization Capability for Cross-Modality.

To verify the generalization capabilities of UMed-LVLM, we train it on single-modality medical images and evaluate it across different modalities. As shown in Table 6, our approach demonstrates better performance in cross-modal generalization compared to other methods. The performance of our model is attributed to our abnormal-aware training method that enhances the model’s capability to adapt to various medical images. The Abnormal-Aware Instruction Tuning and AAR boost the model’s capability to localize abnormalities and diagnose accuracy in medical images. This is particularly important in scenarios where the modalities differ substantially (e.g., CT vs. Gross Pathology).

6 Conclusion

This study introduces UMed-LVLM, a novel Med-LVLM designed to enhance medical diagnosis by the visual localization of abnormalities in medical images. Through a specialized training process involving the collection of a Medical Abnormalities Unveiling dataset and the implementation of Abnormal-Aware Instruction Tuning and Abnormal-Aware Rewarding. Results show UMed-LVLM surpasses existing Med-LVLMs in accurately detecting and interpreting medical anomalies.

The AAR incorporates innovative reward mechanisms that sharpen the model’s focus on abnormal areas, thereby improving diagnostic reliability and interpretability. Furthermore, the in-depth analysis suggests that UMed-LVLM trained in some medical datasets can substantially boost their performance on other datasets, which demonstrates the generalization capability of UMed-LVLM.

Limitations

Our study has two limitations: the availability of annotated medical data and the limited computational resources.

Data Availability. One of the most significant limitations is the scarcity of annotated medical data. High-quality, well-annotated datasets are critical for training and validating machine learning models, particularly in the field of medical research. However, such datasets are often difficult to obtain due to two reasons: Firstly, medical data is sensitive, and its collection and distribution are strictly regulated to protect patient privacy. This makes it challenging to access comprehensive datasets that cover a wide range of medical conditions. Moreover, the process of annotating medical data is both time-consuming and expensive. It requires the expertise of medical professionals, who must carefully review and label each data point to ensure accuracy. This meticulous process significantly limits the quantity and cost of available data.

Limited Computational Resources. The second limitation is the limited computational resources. Recent advancements have led to the development of increasing size of LVLMs, which require substantial computational power to train and deploy effectively. As a result of these computational limitations, we were unable to apply our methodologies to the largest and most complex open-source models currently available. This limits our ability to expand and validate our approach on larger-scale LVLMs.

References

Jean-Baptiste Alayrac, Jeff Donahue, Pauline Luc, Antoine Miech, Iain Barr, Yana Hasson, Karel Lenc, Arthur Mensch, Katherine Millican, Malcolm Reynolds, Roman Ring, Eliza Rutherford, Serkan Cabi, Tengda Han, Zhitao Gong, Sina Samangooei, Marianne Monteiro, Jacob L. Menick, Sebastian Borgeaud, Andy Brock, Aida Nematzadeh, Sahand Sharifzadeh, Mikolaj Binkowski, Ricardo Barreira,

Oriol Vinyals, Andrew Zisserman, and Karén Simonyan. 2022. [Flamingo: a visual language model for few-shot learning](#). In *NeurIPS*.

Jinze Bai, Shuai Bai, Shusheng Yang, Shijie Wang, Sinan Tan, Peng Wang, Junyang Lin, Chang Zhou, and Jingren Zhou. 2023. [Qwen-vl: A frontier large vision-language model with versatile abilities](#). *CoRR*, abs/2308.12966.

Tom B. Brown, Benjamin Mann, Nick Ryder, Melanie Subbiah, Jared Kaplan, Prafulla Dhariwal, Arvind Neelakantan, Pranav Shyam, Girish Sastry, Amanda Askell, Sandhini Agarwal, Ariel Herbert-Voss, Gretchen Krueger, Tom Henighan, Rewon Child, Aditya Ramesh, Daniel M. Ziegler, Jeffrey Wu, Clemens Winter, Christopher Hesse, Mark Chen, Eric Sigler, Mateusz Litwin, Scott Gray, Benjamin Chess, Jack Clark, Christopher Berner, Sam McCandlish, Alec Radford, Ilya Sutskever, and Dario Amodei. 2020. [Language models are few-shot learners](#). In *NeurIPS 2020*.

Yuanjiang Cao, Quan Z. Sheng, Julian J. McAuley, and Lina Yao. 2023. [Reinforcement learning for generative AI: A survey](#). *CoRR*, abs/2308.14328.

Xi Chen, Xiao Wang, Soravit Changpinyo, A. J. Piergiovanni, Piotr Padlewski, Daniel Salz, Sebastian Goodman, Adam Grycner, Basil Mustafa, Lucas Beyer, Alexander Kolesnikov, Joan Puigcerver, Nan Ding, Keran Rong, Hassan Akbari, Gaurav Mishra, Linting Xue, Ashish V. Thapliyal, James Bradbury, and Weicheng Kuo. 2023. [Pali: A jointly-scaled multilingual language-image model](#). In *ICLR 2023*. OpenReview.net.

Wei-Lin Chiang, Zhuohan Li, Zi Lin, Ying Sheng, Zhanghao Wu, Hao Zhang, Lianmin Zheng, Siyuan Zhuang, Yonghao Zhuang, Joseph E Gonzalez, et al. 2023. Vicuna: An open-source chatbot impressing gpt-4 with 90%* chatgpt quality. See <https://vicuna.lmsys.org> (accessed 14 April 2023), 2(3):6.

Paul F. Christiano, Jan Leike, Tom B. Brown, Miljan Martic, Shane Legg, and Dario Amodei. 2017. [Deep reinforcement learning from human preferences](#). In *Advances in Neural Information Processing Systems 30: Annual Conference on Neural Information Processing Systems 2017, December 4-9, 2017, Long Beach, CA, USA*, pages 4299–4307.

Alexey Dosovitskiy, Lucas Beyer, Alexander Kolesnikov, Dirk Weissenborn, Xiaohua Zhai, Thomas Unterthiner, Mostafa Dehghani, Matthias Minderer, Georg Heigold, Sylvain Gelly, Jakob Uszkoreit, and Neil Houlsby. 2021. [An image is worth 16x16 words: Transformers for image recognition at scale](#). In *ICLR 2021*. OpenReview.net.

Weihao Gao, Zhuo Deng, Zhiyuan Niu, Fujun Rong, Chucheng Chen, Zheng Gong, Wenze Zhang, Daimin Xiao, Fang Li, Zhenjie Cao, Zhaoyi Ma, Wenbin Wei, and Lan Ma. 2023. [Ophglm: Training an ophthalmology large language-and-vision assistant based on instructions and dialogue](#). *CoRR*, abs/2306.12174.

- Qiushan Guo, Shalini De Mello, Hongxu Yin, Wonmin Byeon, Ka Chun Cheung, Yizhou Yu, Ping Luo, and Sifei Liu. 2024. [Regionpt: Towards region understanding vision language model](#). *CoRR*, abs/2403.02330.
- Sahar Kazemzadeh, Vicente Ordonez, Mark Matten, and Tamara L. Berg. 2014. [Referitgame: Referring to objects in photographs of natural scenes](#). In *EMNLP 2014*, pages 787–798. ACL.
- Diederik P. Kingma and Jimmy Ba. 2015. [Adam: A method for stochastic optimization](#). In *ICLR 2015*.
- Ranjay Krishna, Yuke Zhu, Oliver Groth, Justin Johnson, Kenji Hata, Joshua Kravitz, Stephanie Chen, Yannis Kalantidis, Li-Jia Li, David A. Shamma, Michael S. Bernstein, and Li Fei-Fei. 2017. [Visual genome: Connecting language and vision using crowdsourced dense image annotations](#). *Int. J. Comput. Vis.*, 123(1):32–73.
- Chunyuan Li, Cliff Wong, Sheng Zhang, Naoto Usuyama, Haotian Liu, Jianwei Yang, Tristan Naumann, Hoifung Poon, and Jianfeng Gao. 2023a. [Llava-med: Training a large language-and-vision assistant for biomedicine in one day](#). In *NeurIPS 2023*.
- Junnan Li, Dongxu Li, Silvio Savarese, and Steven C. H. Hoi. 2023b. [BLIP-2: bootstrapping language-image pre-training with frozen image encoders and large language models](#). In *ICML 2023*, volume 202 of *Proceedings of Machine Learning Research*, pages 19730–19742. PMLR.
- Haotian Liu, Chunyuan Li, Yuheng Li, and Yong Jae Lee. 2023a. [Improved baselines with visual instruction tuning](#). *CoRR*, abs/2310.03744.
- Haotian Liu, Chunyuan Li, Qingyang Wu, and Yong Jae Lee. 2023b. [Visual instruction tuning](#). In *NeurIPS 2023*.
- Junling Liu, Ziming Wang, Qichen Ye, Dading Chong, Peilin Zhou, and Yining Hua. 2023c. [Qilin-med-vl: Towards chinese large vision-language model for general healthcare](#). *CoRR*, abs/2310.17956.
- Yun Liu, Yu-Huan Wu, Yunfeng Ban, Huifang Wang, and Ming-Ming Cheng. 2020. [Rethinking computer-aided tuberculosis diagnosis](#). In *CVPR 2020*, pages 2643–2652. Computer Vision Foundation / IEEE.
- Yun Luo, Zhen Yang, Fandong Meng, Yafu Li, Jie Zhou, and Yue Zhang. 2023. [An empirical study of catastrophic forgetting in large language models during continual fine-tuning](#). *CoRR*, abs/2308.08747.
- Kenneth Marino, Mohammad Rastegari, Ali Farhadi, and Roozbeh Mottaghi. 2019. [OK-VQA: A visual question answering benchmark requiring external knowledge](#). In *CVPR 2019*, pages 3195–3204. Computer Vision Foundation / IEEE.
- Anand Mishra, Shashank Shekhar, Ajeet Kumar Singh, and Anirban Chakraborty. 2019. [OCR-VQA: visual question answering by reading text in images](#). In *2019 International Conference on Document Analysis and Recognition, ICDAR 2019, Sydney, Australia, September 20-25, 2019*, pages 947–952. IEEE.
- Volodymyr Mnih, Adrià Puigdomènech Badia, Mehdi Mirza, Alex Graves, Timothy P. Lillicrap, Tim Harley, David Silver, and Koray Kavukcuoglu. 2016. [Asynchronous methods for deep reinforcement learning](#). In *ICML 2016*, volume 48 of *JMLR Workshop and Conference Proceedings*, pages 1928–1937. JMLR.org.
- Volodymyr Mnih, Koray Kavukcuoglu, David Silver, Andrei A. Rusu, Joel Veness, Marc G. Bellemare, Alex Graves, Martin A. Riedmiller, Andreas Fidjeland, Georg Ostrovski, Stig Petersen, Charles Beattie, Amir Sadik, Ioannis Antonoglou, Helen King, Dharmashan Kumaran, Daan Wierstra, Shane Legg, and Demis Hassabis. 2015. [Human-level control through deep reinforcement learning](#). *Nat.*, 518(7540):529–533.
- Michael Moor, Qian Huang, Shirley Wu, Michihiro Yasunaga, Yash Dalmia, Jure Leskovec, Cyril Zarka, Eduardo Pontes Reis, and Pranav Rajpurkar. 2023. [Med-flamingo: a multimodal medical few-shot learner](#). In *MLAH@NeurIPS 2023*, volume 225 of *Proceedings of Machine Learning Research*, pages 353–367. PMLR.
- Reiichiro Nakano, Jacob Hilton, Suchir Balaji, Jeff Wu, Long Ouyang, Christina Kim, Christopher Hesse, Shantanu Jain, Vineet Kosaraju, William Saunders, Xu Jiang, Karl Cobbe, Tyna Eloundou, Gretchen Krueger, Kevin Button, Matthew Knight, Benjamin Chess, and John Schulman. 2021. [Webgpt: Browser-assisted question-answering with human feedback](#). *CoRR*, abs/2112.09332.
- OpenAI. 2023a. [GPT-4 technical report](#). *CoRR*, abs/2303.08774.
- OpenAI. 2023b. [Gpt-4v\(ision\) system card](#).
- Long Ouyang, Jeffrey Wu, Xu Jiang, Diogo Almeida, Carroll L. Wainwright, Pamela Mishkin, Chong Zhang, Sandhini Agarwal, Katarina Slama, Alex Ray, John Schulman, Jacob Hilton, Fraser Kelton, Luke Miller, Maddie Simens, Amanda Askell, Peter Welinder, Paul F. Christiano, Jan Leike, and Ryan Lowe. 2022. [Training language models to follow instructions with human feedback](#). In *NeurIPS 2022*.
- Konstantin Pogorelov, Kristin Ranheim Randel, Carsten Griwodz, Sigrun Losada Eskeland, Thomas de Lange, Dag Johansen, Concetto Spampinato, Duc-Tien Dang-Nguyen, Mathias Lux, Peter Thelin Schmidt, Michael Riegler, and Pål Halvorsen. 2017. [KVASIR: A multi-class image dataset for computer aided gastrointestinal disease detection](#). In *Proceedings of the 8th ACM on Multimedia Systems Conference, MM-Sys 2017, Taipei, Taiwan, June 20-23, 2017*, pages 164–169. ACM.

- Ziyuan Qin, Huahui Yi, Qicheng Lao, and Kang Li. 2023. [MEDICAL IMAGE UNDERSTANDING WITH PRETRAINED VISION LANGUAGE MODELS: A COMPREHENSIVE STUDY](#). In *ICLR 2023*. OpenReview.net.
- Alec Radford, Jong Wook Kim, Chris Hallacy, Aditya Ramesh, Gabriel Goh, Sandhini Agarwal, Girish Sastry, Amanda Askell, Pamela Mishkin, Jack Clark, Gretchen Krueger, and Ilya Sutskever. 2021. [Learning transferable visual models from natural language supervision](#). In *ICML 2021*, volume 139 of *Proceedings of Machine Learning Research*, pages 8748–8763. PMLR.
- Kanchana Ranasinghe, Satya Narayan Shukla, Omid Poursaeed, Michael S. Ryoo, and Tsung-Yu Lin. 2024. [Learning to localize objects improves spatial reasoning in visual-llms](#). In *IEEE/CVF Conference on Computer Vision and Pattern Recognition, CVPR 2024, Seattle, WA, USA, June 16-22, 2024*, pages 12977–12987. IEEE.
- John Schulman, Sergey Levine, Pieter Abbeel, Michael I. Jordan, and Philipp Moritz. 2015. [Trust region policy optimization](#). In *ICML 2015*, volume 37 of *JMLR Workshop and Conference Proceedings*, pages 1889–1897. JMLR.org.
- John Schulman, Filip Wolski, Prafulla Dhariwal, Alec Radford, and Oleg Klimov. 2017. [Proximal policy optimization algorithms](#). *CoRR*, abs/1707.06347.
- Dustin Schwenk, Apoorv Khandelwal, Christopher Clark, Kenneth Marino, and Roozbeh Mottaghi. 2022. [A-OKVQA: A benchmark for visual question answering using world knowledge](#). In *ECCV 2022*, volume 13668 of *Lecture Notes in Computer Science*, pages 146–162. Springer.
- Chang Shu, Baian Chen, Fangyu Liu, Zihao Fu, Ehsan Shareghi, and Nigel Collier. 2023. [Visual medalpaca: A parameter-efficient biomedical llm with visual capabilities](#).
- Oleksii Sidorov, Ronghang Hu, Marcus Rohrbach, and Amanpreet Singh. 2020. [Textcaps: A dataset for image captioning with reading comprehension](#). In *ECCV 2020*, volume 12347 of *Lecture Notes in Computer Science*, pages 742–758. Springer.
- Nisan Stiennon, Long Ouyang, Jeff Wu, Daniel M. Ziegler, Ryan Lowe, Chelsea Voss, Alec Radford, Dario Amodei, and Paul F. Christiano. 2020. [Learning to summarize from human feedback](#). *CoRR*, abs/2009.01325.
- Richard S. Sutton and Andrew G. Barto. 1998. [Reinforcement learning - an introduction](#). Adaptive computation and machine learning. MIT Press.
- TEZ. 2023. [Tez_roi_aug dataset](#). https://universe.roboflow.com/tez-nwxf5/tez_roi_aug. Visited on 2024-05-21.
- Omkar Thawakar, Abdelrahman Shaker, Sahal Shaji Mullappilly, Hisham Cholakkal, Rao Muhammad Anwer, Salman H. Khan, Jorma Laaksonen, and Fahad Shahbaz Khan. 2023. [Xraygpt: Chest radiographs summarization using medical vision-language models](#). *CoRR*, abs/2306.07971.
- Guangyu Wang, Guoxing Yang, Zongxin Du, Longjun Fan, and Xiaohu Li. 2023. [Clinicalgpt: Large language models finetuned with diverse medical data and comprehensive evaluation](#). *CoRR*, abs/2306.09968.
- Xiaosong Wang, Yifan Peng, Le Lu, Zhiyong Lu, Mohammadhadi Bagheri, and Ronald M. Summers. 2017. [Chestx-ray8: Hospital-scale chest x-ray database and benchmarks on weakly-supervised classification and localization of common thorax diseases](#). In *CVPR 2017*, pages 3462–3471. IEEE Computer Society.
- Zifeng Wang, Zhenbang Wu, Dinesh Agarwal, and Jimeng Sun. 2022. [Medclip: Contrastive learning from unpaired medical images and text](#). In *EMNLP 2022*, pages 3876–3887. Association for Computational Linguistics.
- Jason Wei, Maarten Bosma, Vincent Y. Zhao, Kelvin Guu, Adams Wei Yu, Brian Lester, Nan Du, Andrew M. Dai, and Quoc V. Le. 2022. [Finetuned language models are zero-shot learners](#). In *ICLR 2022*. OpenReview.net.
- Chaoyi Wu, Jiayu Lei, Qiaoyu Zheng, Weike Zhao, Weixiong Lin, Xiaoman Zhang, Xiao Zhou, Ziheng Zhao, Ya Zhang, Yanfeng Wang, and Weidi Xie. 2023. [Can gpt-4v\(ision\) serve medical applications? case studies on GPT-4V for multimodal medical diagnosis](#). *CoRR*, abs/2310.09909.
- Shao-Hong Wu, Wen-Juan Tong, Ming-De Li, Hang-Tong Hu, Xiao-Zhou Lu, Ze-Rong Huang, Xin-Xin Lin, Rui-Fang Lu, Ming-De Lu, Li-Da Chen, and Wei Wang. 2024. [Collaborative enhancement of consistency and accuracy in us diagnosis of thyroid nodules using large language models](#). *Radiology*, 310(3):e232255. PMID: 38470237.
- Ke Yan, Xiaosong Wang, Le Lu, and Ronald M. Summers. 2017. [Deeplesion: Automated deep mining, categorization and detection of significant radiology image findings using large-scale clinical lesion annotations](#). *CoRR*, abs/1710.01766.
- Songhua Yang, Hanjie Zhao, Senbin Zhu, Guangyu Zhou, Hongfei Xu, Yuxiang Jia, and Hongying Zan. 2024. [Zhongjing: Enhancing the chinese medical capabilities of large language model through expert feedback and real-world multi-turn dialogue](#). In *AAAI 2024*, pages 19368–19376. AAAI Press.
- Qinghao Ye, Haiyang Xu, Guohai Xu, Jiabo Ye, Ming Yan, Yiyang Zhou, Junyang Wang, Anwen Hu, Pengcheng Shi, Yaya Shi, Chenliang Li, Yuanhong Xu, Hehong Chen, Junfeng Tian, Qian Qi, Ji Zhang, and Fei Huang. 2023. [mplug-owl: Modularization](#)

- empowers large language models with multimodality. *CoRR*, abs/2304.14178.
- Shukang Yin, Chaoyou Fu, Sirui Zhao, Tong Xu, Hao Wang, Dianbo Sui, Yunhang Shen, Ke Li, Xing Sun, and Enhong Chen. 2023. **Woodpecker: Hallucination correction for multimodal large language models**. *CoRR*, abs/2310.16045.
- Tianyu Yu, Yuan Yao, Haoye Zhang, Taiwen He, Yifeng Han, Ganqu Cui, Jinyi Hu, Zhiyuan Liu, Hai-Tao Zheng, and Maosong Sun. 2024. **RLHF-V: towards trustworthy mllms via behavior alignment from fine-grained correctional human feedback**. In *IEEE/CVF Conference on Computer Vision and Pattern Recognition, CVPR 2024, Seattle, WA, USA, June 16-22, 2024*, pages 13807–13816. IEEE.
- Oliver Zhang, Jean-Benoit Delbrouck, and Daniel L. Rubin. 2021. **Out of distribution detection for medical images**. In *PIPPi 2021*, volume 12959 of *Lecture Notes in Computer Science*, pages 102–111. Springer.
- Xiaoman Zhang, Chaoyi Wu, Ziheng Zhao, Weixiong Lin, Ya Zhang, Yanfeng Wang, and Weidi Xie. 2023a. **PMC-VQA: visual instruction tuning for medical visual question answering**. *CoRR*, abs/2305.10415.
- Xiaoman Zhang, Chaoyi Wu, Ziheng Zhao, Weixiong Lin, Ya Zhang, Yanfeng Wang, and Weidi Xie. 2023b. **Pmc-vqa: Visual instruction tuning for medical visual question answering**. *arXiv preprint arXiv:2305.10415*.
- Chunting Zhou, Pengfei Liu, Puxin Xu, Srinivasan Iyer, Jiao Sun, Yuning Mao, Xuezhe Ma, Avia Efrat, Ping Yu, Lili Yu, Susan Zhang, Gargi Ghosh, Mike Lewis, Luke Zettlemoyer, and Omer Levy. 2023. **LIMA: less is more for alignment**. In *Advances in Neural Information Processing Systems 36: Annual Conference on Neural Information Processing Systems 2023, NeurIPS 2023, New Orleans, LA, USA, December 10 - 16, 2023*.
- Yucheng Zhou, Xiang Li, Qianning Wang, and Jianbing Shen. 2024a. **Visual in-context learning for large vision-language models**. In *Findings of the Association for Computational Linguistics, ACL 2024, Bangkok, Thailand and virtual meeting, August 11-16, 2024*, pages 15890–15902. Association for Computational Linguistics.
- Yucheng Zhou, Zhi Rao, Jun Wan, and Jianbing Shen. 2024b. **Rethinking visual dependency in long-context reasoning for large vision-language models**. *arXiv preprint arXiv:2410.19732*.
- Deyao Zhu, Jun Chen, Xiaoqian Shen, Xiang Li, and Mohamed Elhoseiny. 2024. **Minigt-4: Enhancing vision-language understanding with advanced large language models**. In *ICLR 2024*. OpenReview.net.

A Related Work

A.1 Large Vision-Language Models

Recently, there have been remarkable advancements within the domain of LVLMs (Alayrac et al., 2022; Chen et al., 2023; Zhou et al., 2024b,a). These models effectively bridge the gap between visual comprehension and contextual language understanding, presenting a robust solution for reconciling disparities between visual and textual data, and thereby, enhancing their capacity to address various vision-language tasks. By pre-training on image-text pairs, CLIP (Radford et al., 2021) achieved zero-shot transfer to diverse computer vision tasks without requiring task-specific training. In contrast, BLIP-2 (Li et al., 2023b) employed frozen pre-trained image encoders and LLMs to bridge the modality gap, achieving effective representation and generative learning. The introduction of GPT-4 (OpenAI, 2023a) ushered in a new era of LVLMs (Zhu et al., 2024; Ye et al., 2023; Bai et al., 2023). LLaVA (Liu et al., 2023b) leveraged a language-only GPT-4 to generate high-quality multimodal instruction data effectively. Notably, LLaVA demonstrated exceptional chat capabilities, even when provided with novel images and instructions. The improved version LLaVA (Liu et al., 2023a) elevated its performance by incorporating academic-task-oriented VQA datasets (Marino et al., 2019; Mishra et al., 2019; Sidorov et al., 2020; Schwenk et al., 2022) and simple response formatting prompts, thus establishing stronger baselines. It is worth mentioning that the inclusion of region-level VQA datasets (Kazemzadeh et al., 2014; Krishna et al., 2017) could significantly enhance the model’s ability to localize fine-grained visual details precisely.

A.2 Large Medical Vision-Language Models

Medical applications of LVLMs require the utilization of specialized models that possess the ability to interpret medical images. LLaVA-Med (Li et al., 2023a) extended the capabilities of LLaVA (Liu et al., 2023b) to the medical domain with excellent multimodal dialogue capabilities. Unlike Visual Med-Alpaca (Shu et al., 2023), which connected image captioning models with an LLM and employed a classifier for model assignment, LLaVA-Med is an end-to-end model specifically designed for the medical field. In specific medical domains, LVLMs also play a significant role. In ophthalmology, OphGLM (Gao et al., 2023) combined

visual and language capabilities to provide comprehensive ophthalmic assistance. To solve open-ended questions about chest radiographs, XrayGPT (Thawakar et al., 2023) effectively aligned the medical visual encoder (Wang et al., 2022) with a fine-tuned large language model (Chiang et al., 2023) by employing a straightforward linear transformation. The scarcity of non-English language models prompted the introduction of Qilin-Med-VL (Liu et al., 2023c) as the Chinese large vision-language model that combines a pre-trained Vision Transformer (Dosovitskiy et al., 2021) with a foundational Large Language Model. Observations in (Wu et al., 2023) indicated that although GPT-4V performs well in differentiating medical image modalities and anatomy, it still has difficulties in disease diagnosis and generating comprehensive reports. More specifically, GPT-4V demonstrates inadequate performance in accurately identifying the structures or abnormalities in medical images.

A.3 Reinforcement Learning for Large Language Models

Reinforcement Learning (RL) can be defined as a training paradigm that could learn from interactions with environments (Sutton and Barto, 1998). Following the inception of RL, a multitude of approaches have been proposed, some of the more widely used are Q-learning (Mnih et al., 2015), Trust Region Policy Optimization (TRPO) (Schulman et al., 2015), Asynchronous Advantage Actor-critic (A3C) (Mnih et al., 2016) and Proximal Policy Optimization (PPO) (Schulman et al., 2017). Different from the distribution modeling objective of supervised and unsupervised learning, RL is more flexible in terms of reward functions, which facilitates the application of RL methods to generative AI models (Cao et al., 2023). In the domain of LLMs, RL can be a vital technique for their development to unlock significant potential. As a successful application of RL combined to LLM, WebGPT (Nakano et al., 2021) optimized the reward function through RL and rejection sampling with the aim of improving its behavior. Another illustrative example of employing RL to LLM is InstructGPT (Ouyang et al., 2022), which used methodology of both reinforcement learning with human feedback (RLHF (Stiennon et al., 2020; Christiano et al., 2017)) and PPO to proficiently fine-tune GPT-3 (Brown et al., 2020), thereby empowering it to follow a diverse range of written instructions. It is worth noting that, in addition to the realm of

Table 7: Specific details of the segments used from datasets.

Dataset	Type	Class	Train	Test	Total
DeepLesion	CT	9	1,584	396	1,980
KidneyStone	CT	1	843	211	1,054
NIH	X-ray	14	787	197	984
TBX11K	X-ray	1	639	160	799
KVASIR	Pathology	1	800	200	1,000
Total	3	26	4,653	1,164	5,817

general LLMs, there are already some examples of medical LLMs that make use of RL. Some brilliant works about medical LLMs like ClinicalGPT (Wang et al., 2023) and Zhongjing (Yang et al., 2024) also utilized RL to reduce the bias of LLM and improve performance. While RL has been extensively harnessed in LLMs and medical LLMs, its potential for enhancing capacity of identifying and describing abnormalities within medical images remains to be explored.

B MAU Dataset

The details of dataset are shown in Table 7. This dataset encompasses five distinct sub-datasets, namely DeepLesion (Yan et al., 2017), KidneyStone (TEZ, 2023), NIH (Wang et al., 2017), TBX11K (Liu et al., 2020), and KVASIR (Pogorelov et al., 2017), each originating from diverse sources. DeepLesion consists of 32,120 axial CT slices featuring eight different types of abnormalities such as lesions in the lungs, abdomen, mediastinum, liver, pelvis, soft tissue, kidneys, and bones. The KidneyStone dataset contains 1,300 renal CT scans depicting various kidney stones, covering a range of sizes, shapes, and locations within the urinary system. The NIH dataset includes 112,120 chest X-ray images, covering 14 different pathological categories including, but not limited to, pneumonia, tuberculosis, lung cancer, pulmonary edema, and pulmonary fibrosis. The TBX11K dataset comprises 11,200 chest X-ray images focused on the classification and detection of tuberculosis (TB), categorizing images into healthy, sick but non-TB, active TB, latent TB, and indeterminate TB. The KVASIR dataset contains 8,000 endoscopic images of the gastrointestinal (GI) tract, focusing on GI diseases with eight different types of abnormalities such as polyps, tumors, or other abnormal tissues. As shown in Figure 6, we present some examples from the MAU dataset.

C Implementation Details

In the experiments, we employ MedVInt (Zhang et al., 2023b) to initialize our model. During the instruction tuning phase, we employed an Adam optimizer (Kingma and Ba, 2015) with a learning rate of 1×10^{-5} , weight decay of 0.01 and a batch size of 128. We train the model on four epochs, utilizing a linear decay strategy for the learning rate. For the AAR method, we set $\gamma = 0.99$, $c_1 = 0.5$, $c_2 = 0.5$, and $c_3 = 0.01$. We used an Adam optimizer with a learning rate of 1×10^{-6} and a batch size of 16, training the model for one epoch. To enhance the diversity of sampling responses, we set the number of sampling candidates to eight and decoded the model with a temperature of 0.9 and a probability threshold (p) of 0.9. Our training was conducted on an NVIDIA H800 GPU.

D Large Vision-Language Models

In this study, we evaluate a variety of large vision-language models (LVLMs) and medical LVLMs (Med-LVLMs), including general-purpose models such as MiniGPT-4 (Zhu et al., 2024), mPLUG-Owl (Ye et al., 2023), LLaVA (Liu et al., 2023b), Qwen-VL (Bai et al., 2023), and specialized models like Med-LVLMs, including XrayGPT (Thawakar et al., 2023), LLaVA-Med (Li et al., 2023a), Med-Flamingo (Moor et al., 2023), and MedVInt (Zhang et al., 2023a). While MiniGPT-4, mPLUG-Owl, LLaVA, and Qwen-VL are designed for general visual tasks, LLaVA-Med, XrayGPT, Med-Flamingo, and MedVInt are specifically optimized for the medical domain. These models generally follow a two-stage training process. In the first stage, they align features using large-scale vision-language datasets, while the second stage fine-tunes the model on instruction-following datasets. In our experiments, we extended this approach by further training our model on the MAU dataset using Instruction Tuning and ARRL methods, building on the MedVInt framework. For comparison, we also evaluated GPT-4V (OpenAI, 2023b), which was used in inference mode without additional training due to its closed source.

E Case Study

As shown in Figure 5, we randomly sample examples to compare our method (i.e., UMed-LVLM) and GPT-4V. For instance, in the first medical image, a chest X-ray, the UMed-LVLM identified



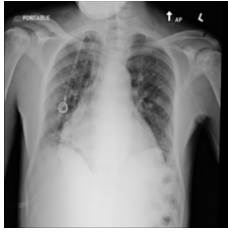
	UMed-LVLM	GPT-4V
	<p>Based on the provided information, the lesion identified within the bounding box coordinates [bbox_start] 0.364, 0.218, 0.184, 0.144 [bbox_end] is located in the upper lobe of the lung. The chest radiograph reveals signs consistent with pulmonary tuberculosis.</p>	<p>The analysis of the chest X-ray has identified a large area which has been highlighted with a bounding box. However, the bounding box covers the entire image, which indicates that the thresholding method used may not have been appropriate for identifying specific abnormalities in this X-ray. It's important to note that accurately localizing abnormalities in medical images typically requires expert medical knowledge and often advanced image processing techniques beyond simple thresholding. For a definitive analysis, a radiologist or a trained medical professional would need to review the image. With the method used, I was unable to localize a specific abnormality.</p>
IoU	0.46	0
	<p>The lesion is enclosed within a bounding box with coordinates [bbox_start] 0.52, 0.374, 0.388, 0.464 [bbox_end]. The image depicts a polyp within the gastrointestinal tract, indicating an abnormal growth. This polyp requires further evaluation by a medical professional to assess its characteristics and determine the appropriate course of treatment.</p>	<p>The image appears to be a clinical photograph from an endoscopy. There is a prominent growth in the image with the following coordinates: [0.2, 0.3, 0.6, 0.3], which seems to be the focal point of concern. However, as an AI, I'm not able to provide medical advice or diagnoses. For a definitive assessment, the image should be examined by a medical professional who can provide an accurate diagnosis and advice. If this is a personal medical image, please consult with your healthcare provider. If this image is for educational or research purposes, you may want to have it reviewed by a medical expert in the field of gastroenterology.</p>
IoU	0.44	0.20

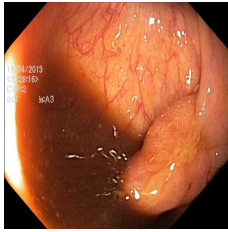
Figure 5: The comparison of diagnosis results between UMed-LVLM and GPT-4V on randomly sampled samples.

a suspicious lesion in the upper lobe of the lung. Despite the IoU score being moderate, the system was able to localize the abnormality, which corresponds to clinical findings consistent with pulmonary tuberculosis. In contrast, GPT-4V failed to localize the abnormality, as it deemed the method it used not suitable for pinpointing specific abnormalities. Similarly, in the gastrointestinal tract image, our UMed-LVLM delineated a polyp with an IoU score of 0.44, suggesting the presence of abnormal growth, whereas GPT-4V with IoU of 0.20. These show our model's proficiency in localizing medical abnormalities.



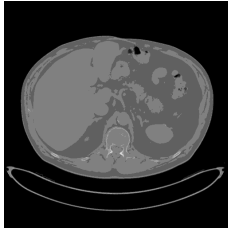
Q: What can you deduce from the provided medical image and describe the anomaly's location?

A: The bounding box of the lesion, marked to delineate the enlarged cardiac silhouette, is defined as follows: [bbox_start] 0.214, 0.381, 0.525, 0.406 [bbox_end]. This area highlights the region within the chest cavity where the heart appears enlarged. Cardiomegaly can have several potential implications, including symptoms such as shortness of breath, fatigue, and swelling of the legs. It may be indicative of underlying conditions such as hypertension, heart valve disease, or cardiomyopathy, necessitating further diagnostic evaluation and appropriate management.



Q: Based on the given information, can you discuss the presence of an anomaly in the medical image and where it is situated?

A: As indicated by the coordinates [bbox_start] 0.493, 0.402, 0.449, 0.553 [bbox_end], the polyp is located within the intestinal lumen. This places the lesion approximately at the center-right of the image. Polyps in the colon can be asymptomatic but may cause symptoms like rectal bleeding, changes in bowel habits, and abdominal pain. The primary concern is that some polyps can develop into colorectal cancer if left untreated. A biopsy is recommended to determine if the polyp is benign or malignant, and regular follow-up colonoscopies may be necessary to monitor for the development of additional polyps.



Q: What can you discern from the provided information about the anomaly within this medical image?

A: Upon reviewing the abdominal CT scan, an abnormal area was identified within the abdomen. The specific region of interest is marked by the following bounding box coordinates:
 - **Lesion Area:** [bbox_start] 0.469, 0.422, 0.033, 0.052 [bbox_end]
 This indicates that the lesion starts at approximately 46.9% from the left edge and 42.2% from the top edge of the image. The lesion spans 3.3% of the image width and 5.2% of the image height.
 The presence of a lesion in the abdominal region, as identified in the CT scan, may indicate a variety of conditions ranging from benign cysts to malignant tumors. Further evaluation by a specialist is necessary to determine the exact nature of the anomaly and to assess any related symptoms or health implications. A biopsy or additional imaging may be required for a definitive diagnosis.



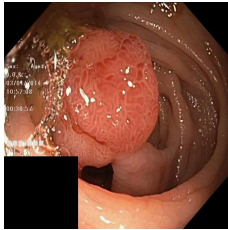
Q: Based on the given details, can you discuss the presence of an abnormality in the medical image and provide insights into where it is located?

A: The pleural thickening is located within the region marked as [bbox_start] 0.623, 0.418, 0.127, 0.151 [bbox_end]. This bounding box indicates the specific area within the right hemithorax where the anomaly is present. Pleural thickening can be indicative of chronic inflammation, fibrosis, or pleural disease. The presence of this thickening suggests the possibility of underlying conditions such as chronic infection, exposure to asbestos, or pleural malignancy. Further evaluation with a CT scan is recommended for better characterization and to rule out other potential underlying pathologies like pleural effusion or malignancy.



Q: Can you deduce any information about the anomaly's location and features within the medical image?

A: The anomaly detected in the CT scan is located in the abdominal region. The specific area of the lesion is identified within the coordinates:
 - [bbox_start] 0.41, 0.409, 0.109, 0.125 [bbox_end]
 - This bounding box indicates the top-left corner at (0.41, 0.409) and spans a width of 0.109 and a height of 0.125 in the normalized coordinate system of the image.
 - The abnormality's location in the abdomen could potentially relate to various symptoms such as abdominal pain, bloating, or changes in bowel habits. Further evaluation is necessary to determine the exact nature and implications of this anomaly.



Q: What can you infer from the medical image provided and what needs to indicate the anomaly's location?

A: The bounding box coordinates for the polyp's location are [bbox_start] 0.201, 0.105, 0.486, 0.665 [bbox_end]. Polyps are abnormal growths of tissue projecting from a mucous membrane, which can sometimes lead to further complications if not addressed.
 The presence of a polyp could potentially indicate a risk of it being malignant, which might necessitate a biopsy to determine its nature (benign or malignant). Follow-up endoscopic examinations and consultations with a gastroenterologist are recommended to monitor and possibly remove the polyp to prevent any further complications.

Figure 6: Examples in MAU datasets.